ADVANCED MATERIALS TECHNOLOGIES
www.advmattechnol.de

Tough Conductive Organohydrogel for Wearable Sensing in Extreme Environmental Conditions

*Seokkyoon Hong, Taewoong Park, Junsang Lee, Yuhyun Ji, Yumin Dai, Jonghun Yi, Joshua Jeremiah Kim, Dong Rip Kim, and Chi Hwan Lee**

Conductive hydrogels, despite their significant potential, have faced historical limitations including vulnerability to dehydration, degradation of performance at extreme temperatures, and susceptibility to freezing in subzero conditions. Furthermore, the development of hydrogels that are both tough and stretchable, capable of maintaining performance under extreme environmental conditions, has remained a challenging task. Here, an innovative conductive organohydrogel, distinguished by its superior toughness, stretchability, stability in regular ambient conditions, vacuum adaptability, and resistance to extreme temperatures is presented. By implementing a unique dry annealing process during synthesis, the mechanical strength of the organohydrogel has been substantially enhanced, dehydration concerns have been alleviated, and the structural integrity has been reinforced. In addition, the composition of the organohydrogel is specifically engineered to achieve both lasting endurance and sustainable longevity. This study signifies a crucial leap forward in creating high-performing organohydrogels capable of functioning in a wide range of environments and conditions, thereby unlocking an array of adaptable applications.

1. Introduction

Conductive hydrogels, known for their flexibility and stimulus responsiveness, hold significant potential in a variety of applications, extending from wearable sensors to advanced biomedical devices.[1] However, several inherent limitations frequently hamper their practical implementation.[2] For example, traditional conductive hydrogels, which mainly use water as a dispersion medium, display susceptibilities to freezing in subzero temperatures, dehydration in dry climates, and drying out at high temperatures (typically, > 37 °C). These conditions can undermine their mechanical and electrical properties, potentially resulting in material failure. While elastomer encapsulation may slightly decrease water evaporation, it still proves ineffective in preventing freezing under subzero temperatures.[3] Thus, there is a need to develop conductive hydrogels that are intrinsically resistant to drying, freezing, and high temperatures. These redesigned hydrogels should deliver consistent and accurate responses to varying external stimuli across a wide range of challenging environments — cold, dry, hot, or otherwise — to cater to numerous scenarios and diverse environmental conditions. Moreover, the hydrogels should also preserve their stretchability and toughness, especially when subjected to extreme conditions.

Here, we introduce a conductive organohydrogel that exhibits a mechanical strength of 2.6 MPa, a toughness of 30.4 MJ m^{-3}, and a stretchability of > 1000%. Remarkably, it resists freezing,

S. Hong, T. Park, J. Lee, Y. Ji, J. J. Kim, C. H. Lee
Weldon School of Biomedical Engineering
Purdue University
West Lafayette, IN47907, USA
E-mail: lee2270@purdue.edu
J. Lee, J. Yi, D. R. Kim
School of Mechanical Engineering
Hanyang University
Seoul04763, Republic of Korea
Y. Dai, C. H. Lee
School of Materials Engineering
Purdue University
West Lafayette, IN 47907, USA
C. H. Lee
Center for Implantable Devices
West Lafayette, IN47907, USA
C. H. Lee
School of Mechanical Engineering
Purdue University
West Lafayette, IN 47907, USA

The ORCID identification number(s) for the author(s) of this article can be found under https://doi.org/10.1002/admt.202301398

DOI: 10.1002/admt.202301398

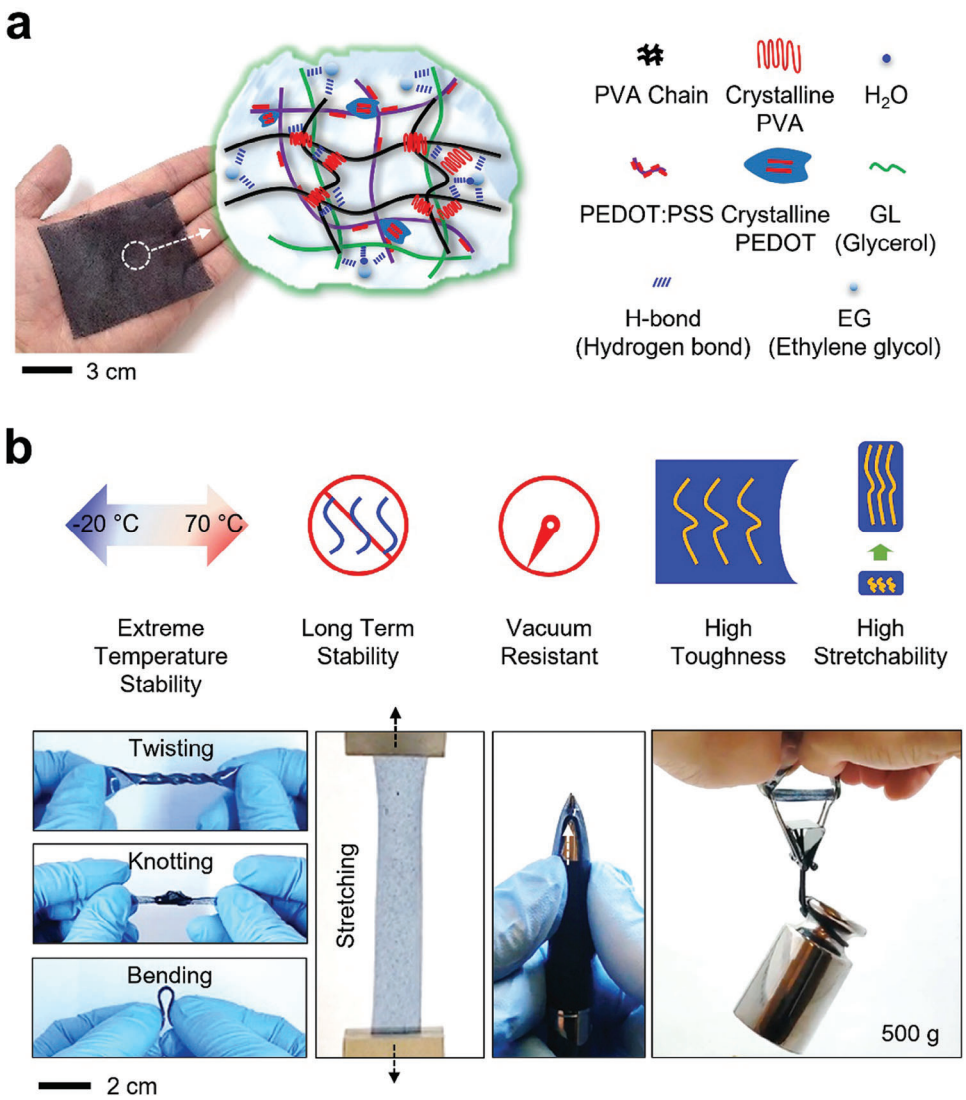

Figure 1. Basic structure and properties. a) Photograph and schematic illustration of the organohydrogel and constituent components. b) Photographs and schematic illustration of the organohydrogel, highlighting its remarkable features such as tolerance to extreme conditions, twisting, knotting, bending, stretching, toughness, and mechanical strength.

drying, and high temperatures while demonstrating excellent stability in ambient conditions and resilience in a vacuum. The organohydrogel is composed of a highly interconnected network of poly(3,4-ethylenedioxythiophene):polystyrene sulfonate (PEDOT:PSS), poly(vinyl alcohol) (PVA), water, ethylene glycol, and glycerol. A unique dry annealing process was employed to enhance its network structure, conferring dehydration resistance and strengthening mechanical properties. This organohydrogel demonstrates a suite of remarkable attributes including high linearity (R^2 > 0.99) over high strain (> 1000%), response/recovery times under 0.4 s without apparent overshoot at 100% strain, and significant durability and cyclical stability in extreme conditions. Our in-depth exploration of its structure-property-performance relationship, compared to contemporary counterparts, provides insightful revelations, as summarized in Table S1 (Supporting Information). We further illustrate its practical applicability with proof-of-concept demonstrations in wearable sensing to monitor joint movements from various body parts.

2. Results and Discussion

2.1. Basic Structure and Properties

Figure 1a presents a photograph and schematic representation of the organohydrogel, which is composed of a densely interconnected network of PEDOT:PSS, PVA, water, ethylene glycol, and glycerol. PEDOT:PSS was chosen for its outstanding electrical conductivity, chemical stability, and aqueous solution processability, while PVA was selected for its cost-effectiveness and strong mechanical properties.[4] The freeze-thawing process of the organohydrogel engenders a crystalline cross-linked PVA domain, facilitating mechanical robustness and stretchability. Concurrently, the PEDOT-rich crystalline domain ensures reliable

electrical performance for strain sensing. Additionally, ethylene glycol resists rigidification upon freezing, allowing the gel to sustain stability at low temperatures. The strong hydrogen bonding between ethylene glycol and water provides greater stability than water-water interactions, effectively preventing solvent freezing at subzero temperatures and disrupting ice crystal lattice formation.[5] The glycerol, due to its excellent hydration retention capability, firmly secures water molecules, preventing easy volatilization and contributing to long-term stability. Specifically, glycerol-water systems have been shown to produce hydrogel networks with greater stability than those formed with pure water.[2e] Moreover, dry annealing promotes the separation of glycerol molecules, leading to the formation of a glycerol film on the hydrogel's surface, which results in fewer surface pores and a denser structure. This further prevents water from evaporating, thus conferring dehydration resistance. The synthesis process began by dissolving 1 g of PVA in a mixture of 4 mL water and 4 mL ethylene glycol at a temperature above 95 °C for over 2 h to obtain a PVA solution. Subsequently, 1 g of PEDOT:PSS was incorporated into the PVA solution and stirred for more than 2 h until homogeneity was achieved. Following this, 2 mL of glycerol was added to the solution and stirred vigorously for over 2 h. The hydrogel was synthesized following a consistent procedure that used 1 g of PVA, 10 mL of water, and 1 g of PEDOT:PSS. The freezing-thawing process of the solution induces mechanical and electrical capabilities, while the dry annealing process enriches the structural characteristics of the organohydrogel. The organohydrogel, due to the anti-freezing effect of organic solvents, retains its stretchability at −20 °C. In contrast, the hydrogel, when frozen at the same temperature, loses its elasticity, making it prone to breakage (Figure S1, Supporting Information). The added solvents enhance not only the anti-freezing properties but also significantly boost its mechanical properties, owing to the augmented intermolecular interactions between the solvent molecules and the PVA chains (Figure S2a, Supporting Information). Upon solvent addition, we observed a notable 181.3% increase in fracture strain and a 13-fold surge in tensile strength compared to the hydrogel (Figure S2b, Supporting Information). The toughness of the organohydrogel saw a remarkable 550-fold increase, highlighting its superior resistance to deformation and fracture under stress. Likewise, the mechanical modulus showcased a 21-fold improvement with solvent incorporation, pointing to a marked elevation in stiffness and rigidity (Figure S2c, Supporting Information). Its electrical conductivity rises with the concentration of PEDOT:PSS, but high PEDOT:PSS concentrations can diminish mechanical properties. This decrease can be attributed to the restricted mobility of PVA chains due to excessive cross-linking and potential PEDOT:PSS aggregation (Figure S3, Supporting Information).[6] As a result, we selected 8 wt.% of PEDOT:PSS as the optimal concentration, balancing between mechanical integrity and conductivity.

Figure 1b presents schematic diagrams and photographs that underscore the impressive features of the organohydrogel, which include resistance to a wide temperature range (from −20 to 70 °C), long-term stability (1-month storage in ambient conditions), resilience in a vacuum (12 psi), superior toughness (30.4 MJ m^{-3}), tensile strength (2.6 MPa), and high stretchability (> 1000%). The organohydrogel maintains its mechanical deformability, such as twisting, knotting, bending, and stretching, across all these environmental conditions. Notably, the organohydrogel remains undamaged when firmly pressed against a sharp tip and can support a weight of 500 g, testaments to its exceptional toughness and mechanical strength. Collectively, these features contribute to the outstanding mechanical stability of the organohydrogel in harsh environments, marking it as a reliable material for sensing applications across a wide range of usage scenarios. Real-time demonstrations showcasing these features are shown in Movie S1 (Supporting Information).

2.2. Dry Annealing

To amplify the structural characteristics of the organohydrogel, we have devised a unique dry annealing process imparting dehydration resistance and boosting its mechanical performance. This process induces the migration of some glycerol molecules, leading to the formation of a glycerol film on the surface. This results in a decreased number of surface pores within the dense matrix, which in turn bolsters dehydration resistance (**Figure 2**a).[7] Furthermore, it promotes tighter molecular chain alignment and significantly diminishes pore size, thereby bolstering its mechanical strength. The accompanying scanning electron microscope (SEM) images illustrate the inner structure of the organohydrogels both pre and post dry-annealing. The dry annealing process commenced with annealing a freeze-thawed specimen (Figure S4, Supporting Information). This sample was meticulously placed between a pair of glass substrates and underwent dry annealing at 60 °C, lasting for more than an hour. Subsequently, one glass substrate was detached, and the exposed side of the sample was targeted in the next dry annealing iteration. The untouched bottom of the specimen was dry annealed by flipping it over. This step-by-step procedure was conducted over 5 times to ensure a comprehensive dry annealing. The ultimate goal was to enhance the organohydrogel's functionality, improving features such as superior toughness and extended storage capacity. This enhancement was realized by densely stacking the molecular chains and forming a glycerol film over its surface. For the attainment of these enhancements, the dry annealing process was undertaken overnight.

Figure 2b reveals a modest 3.7% mass loss in the organohydrogel after dry annealing, a striking contrast to the substantial 46.1% mass loss in the untreated version after 30 days of storage. This distinction underscores the crucial role of the glycerol film plays in enhancing its resistance to drying, thus ensuring its durability and utility. The observed enhancement also underscores the essential contribution of the dry annealing process to the preservation of its structural robustness and functionality. In Figure 2c, a remarkable 147.2% increase in toughness compared to the untreated organohydrogel accentuates its advanced capacity to resist deformation and fracture under stress. A parallel pattern is seen in the mechanical modulus, which demonstrated a significant five-fold enhancement by post-dry annealing, signifying greater stiffness and rigidity. This increase can be attributed to the tighter molecular chain packing, making the material more resistant to deformation. Such observations emphasize the efficacy of the dry annealing process in fostering a condensed molecular arrangement, thereby notably enriching the toughness and mechanical modulus of the organohydrogel.

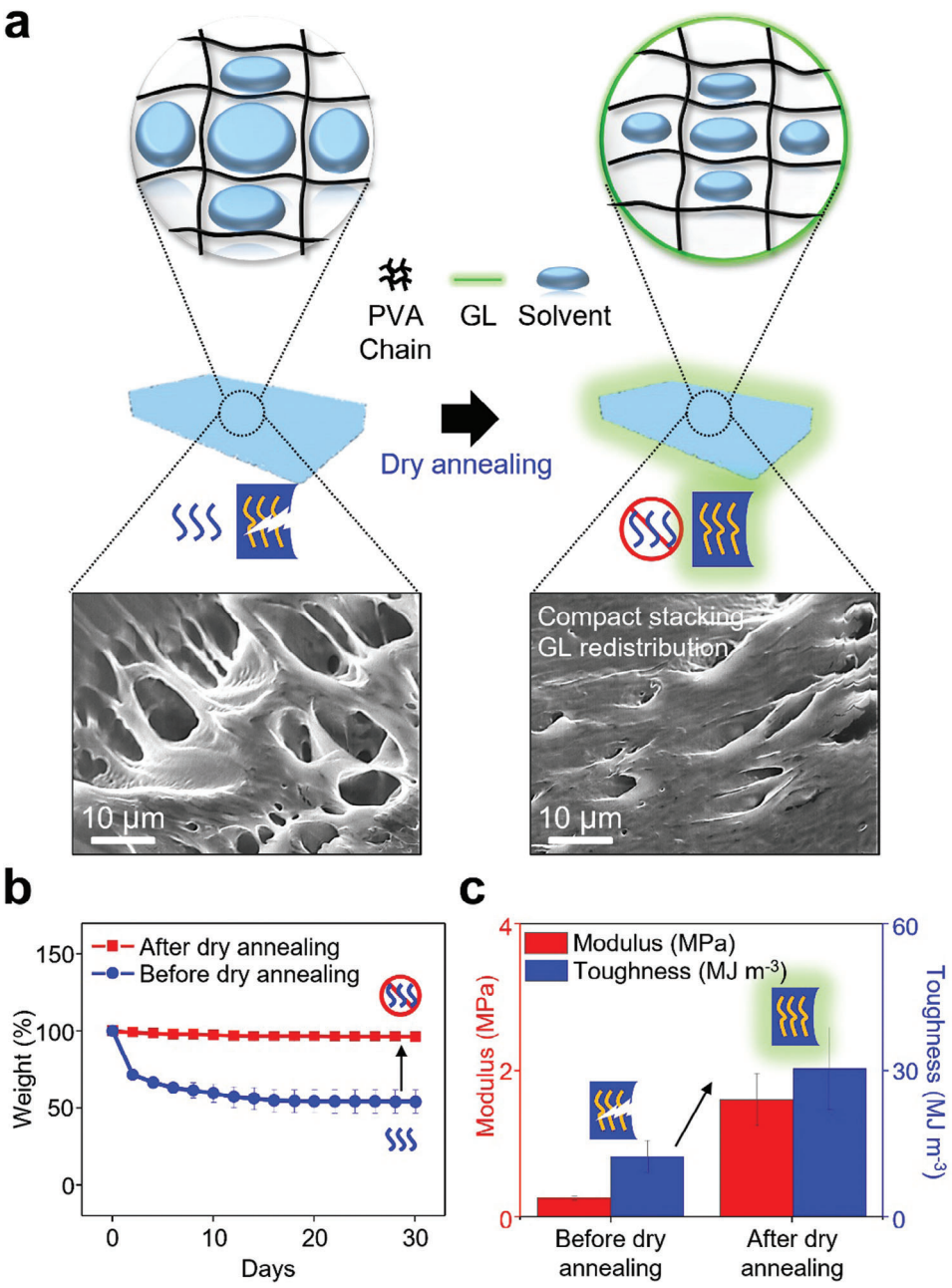

Figure 2. Dry annealing. a) Schematic representation and SEM visuals showcasing the inner structure of organohydrogels pre and post dry-annealing. b) Weight of the organohydrogel before and after dry annealing process. Data presented as mean ± SD, $n = 3$. c) Modulus and toughness of the organohydrogel before and after the dry annealing process. Data presented as mean ± SD, $n = 3$.

2.3. Mechanical Characterization

Figure 3a illustrates the stress-strain curve of the organohydrogel under varying conditions, including low to high temperatures (ranging from −20 to 70 °C), a vacuum (12 psi), and long-term storage (1-month storage in ambient conditions). The organohydrogel began to crumple when the temperature exceeded 120 °C (Figure S5a, Supporting Information). During a 12 h exposure to these conditions, the organohydrogel exhibited negligible weight variation, thus reaffirming its extraordinary solvent retention capabilities. However, the organohydrogel underwent a substantial weight reduction of 61.5% when stored at 120 °C (Figure S5b, Supporting Information).

Even under these demanding circumstances, the organohydrogel exhibits no significant changes to its mechanical properties, showcasing its resilience in various environments. Specifically, the organohydrogel demonstrates high fracture strain and stress under challenging conditions (Figure S6a, Supporting Information) and maintains notable toughness and modulus across various settings (Figure S6b, Supporting Information),

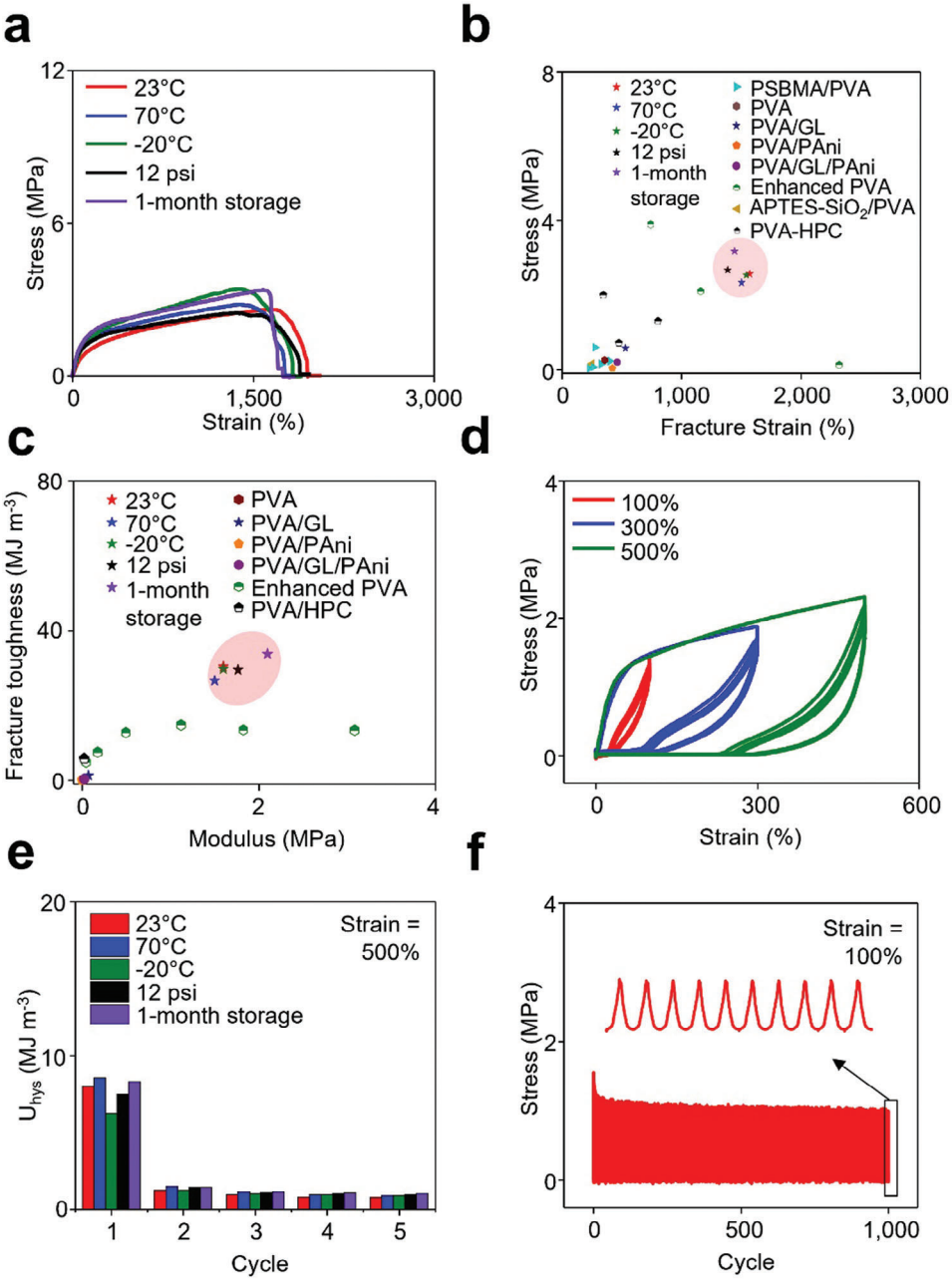

Figure 3. Mechanical characterization. a) Stress-strain curves of the organohydrogel under varied environments. b) Comparison of fracture strain and stress of the organohydrogel with those from prior reports. c) Comparison of modulus and fracture toughness of the organohydrogel with those from prior reports. d) Cyclic stress–strain curves of the organohydrogel at strains of 100%, 300%, and 500%. e) Dissipated energy (U_{hys}) of the organohydrogel at a strain of 500% during different cycles under varied environments. f) Stress of the organohydrogel throughout 1000 stretching-releasing cycles.

outperforming other PVA-based hydrogels (Figure 3b,c).[8] This robustness is primarily attributed to the synergistic influence of: 1) ethylene glycol, which prevents freezing by forming a myriad of hydrogen bonds with water molecules, effectively restraining ice crystal formation at low temperatures; 2) glycerol, with its water-locking effect that provides an anti-drying shield; and 3) the dry annealing process, which not only enhances mechanical performance through closer molecular chain stacking, but also promotes a superior anti-drying effect. This is achieved through the formation of a glycerol film on the surface, due to separation of some glycerol molecules within the organohydrogel, which consequently suppresses water evaporation.

Figure 3d introduces the tensile loading-unloading cyclic tests with strains reaching up to 100%, 300%, and 500%. Evident is a prominent hysteresis loop and energy dissipation (7.96 MJ m^{-3}) during the initial 500% strain loading-unloading cycle, suggestive of its effective energy dissipation capability. Subsequent cyclic loading-unloading tests display a sharp decrease in

hysteresis energy during the immediate second cycle, hinting at its softening after the initial cycle. Crucially, post the first loading cycle, the hysteresis loops obtained from the stress–strain curve maintain consistency, indicative of rapid self-recovery and superior fatigue resistance (Figure 3e). Its stability across these conditions is maintained as the hysteresis loop remains constant (Figure S7, Supporting Information). Notably, the organohydrogel demonstrates swift self-recovery and excellent fatigue resistance under varied conditions, evidenced by the reduced hysteresis energy ($U_{hysteresis}$) in the immediate second cycle (Figure S8, Supporting Information). An increasing trend in hysteresis energy with higher strain levels has been observed, as more cross-linking sites are destroyed, resulting in the dissipation of a larger amount of energy and an increase in the hysteresis loop (Figure S9, Supporting Information). An additional 1000 stretching/releasing cycles at a strain of 100% further underline the exceptional fatigue resistance of the organohydrogel (Figure 3f). These findings remain consistent across different conditions (Figure S10, Supporting Information).

2.4. Electrical Characterization

Figure 4a illustrates the relative resistance change ($\Delta R/R_0$) of the organohydrogel, which shows a high degree of linearity ($R^2 > 0.99$) for an applied strain of up to 1000% across various conditions, such as low to high temperatures (ranging from −20 to 70 °C), vacuum (12 psi), and long-term storage (1-month storage in ambient conditions). This suggests a broad electrical sensing range for the organohydrogel in challenging environments. The high linearity, even under extensive strain, ensures reliable strain sensing without requiring complicated calibration processes (Figure 4b). Figure 4c depicts the $\Delta R/R_0$ of the organohydrogel under 100% strain during loading-unloading cycles. The response patterns remained stable across all the environmental conditions, highlighting its robust endurance. Figure 4d presents the $\Delta R/R_0$ of the organohydrogel under loading-unloading cycles with multiple strains (5%, 10%, 15%, 100%, 200%, and 300%). The consistent response patterns at different strain levels highlight its exceptional stability and continuous response during cyclic loading under varied conditions (Figure S11, Supporting Information). This consistency is maintained across over 1000 cycles of strains exceeding 100%, further attesting to the superior stability with low drift and enduring performance of the organohydrogel without failure (Figure 4e). The slight increase in resistance during the tests arises from the straightening and occasional breakage of the conductive PEDOT chains during the loading-unloading cycles.[9]

Figure 4f presents the $\Delta R/R_0$ of the organohydrogel under varying test rates from 5 to 500 mm min^{-1}. The stable $\Delta R/R_0$ of the organohydrogel under these conditions demonstrates a consistent and reliable response to different external stimuli at rates of 5, 10, 50, 100, and 500 mm min^{-1} (Figure S12, Supporting Information). When subjected to a 100% strain under various conditions, the response and recovery times of the organohydrogel exhibited no significant deviations (Figure S13a, Supporting Information). Its response and recovery times were measured at ≈400 ms (Figure S13b, Supporting Information). Unlike its elastomer-based counterparts, the organohydrogel displayed negligible overshoot or relaxation behavior, a consistency that was maintained across diverse conditions (Figure S14, Supporting Information).[10]

2.5. Proof-of-Concept Demonstrations in Wearable Sensing

The organohydrogel has been effectively used to monitor human movements in real-time, providing essential data concerning the strength, intensity, and consistency of strains exerted on muscles and joints.[11] This information has profound implications in understanding the fields of biomechanics and kinesiology, with potentially significant impacts on numerous facets of healthcare and human performance. Some instances of this include 1) preventing injuries by offering immediate alerts for potentially damaging movements or excessive strain,[12] 2) improved pain management by identifying the underlying causes of chronic pain through persistent observation of muscle and joint forces,[13] and 3) precise gait analysis, which is crucial for diagnosing and treating conditions such as cerebral palsy and Parkinson's disease.[14] To illustrate the potential application of the organohydrogel in motion tracking, we crafted several prototypes designed to measure changes in strain in various body joints, such as fingers, wrists, and elbows, during bending actions from a participant (**Figure 5**). The organohydrogel displayed stable and significant resistance changes in response to deformations caused by a variety of body movements, immediately after exposure to various conditions such as low to high temperatures (ranging from −20 to 70 °C), vacuum (12 psi), and long-term storage (1-month storage in ambient conditions). This performance can be attributed to the unique features of the organohydrogel, including its high toughness, resistance to freezing and drying, resilience to high temperatures, exceptional stability across different environments, robustness in vacuum conditions, and superior stretchability. Realtime demonstrations showcasing these applications are shown in Movie S2 (Supporting Information). Importantly, no adverse skin reactions were observed during these demonstrations (Figure S15, Supporting Information). Specifically, the organohydrogel and 3 M tapes were applied to human skin for ≈10 min and then removed. A control group featured untreated bare skin. Notably, no discernible skin irritation resulted from the application of the organohydrogel. In contrast, the use of 3 M tapes did lead to skin irritation. These observations underscore the biocompatibility of the organohydrogel. Details of the skin irritation tests are described in the Experimental Section.

3. Conclusion

This study presents an organohydrogel of extended environmental tolerance, toughness, and ultra-stretchability. The organohydrogel exhibits an array of commendable properties, such as superior stretchability and high toughness, achieving an ideal balance between its cyclic strain sensing capabilities, high linearity, rapid response and recovery times, and absence of overshoot behavior, all without substantial compromises. The distinctive characteristics of the organohydrogel can be attributed to its unique network structure, which is a result of strong interconnections and dynamic interactions among its components. A crucial step in the manufacturing process, dry annealing, bestows

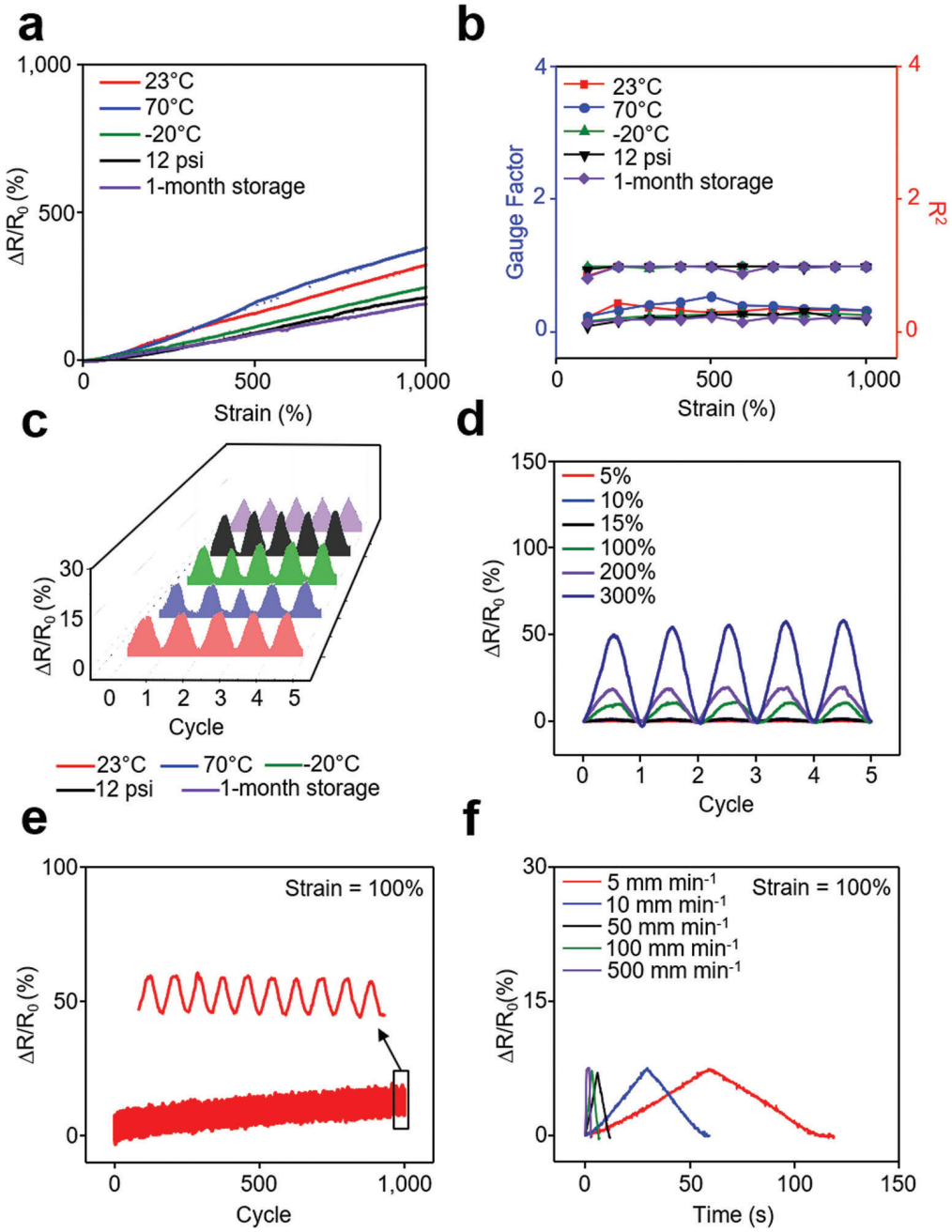

Figure 4. Electrical characterization. a) $\Delta R/R_0$ of the organohydrogel with strain under varied environments. b) Gauge factor and linearity of the organohydrogel up to a strain of 1000% c) $\Delta R/R_0$ of the organohydrogel under loading-unloading cycles at strain of 100% under diverse conditions. d) $\Delta R/R_0$ of the organohydrogel under loading-unloading cycles at strains of 5%, 10%, 15%, 100%, 200% and 300%. e) $\Delta R/R_0$ of the organohydrogel throughout 1000 stretching-releasing cycles with a strain of 100%. f) $\Delta R/R_0$ of the organohydrogel under varying test rates from 5 to 500 mm min^{-1} at a strain of 100%.

the organohydrogel with both anti-drying and high toughness attributes. The organohydrogel synthesized in this study demonstrates reliable performance in monitoring human movements, even in varied and challenging situations. The organohydrogel holds immense potential for use in wearable sensing applications across a variety of environmental conditions. This positions it as a significant catalyst for advancements in diverse sectors, including sports medicine, prosthetics, and robotics.[15]

4. Experimental Section

Materials: The PVA (Mw: 146 000–186 000), PEDOT:PSS, and glycerol were purchased from Sigma–Aldrich, and the ethylene glycol was purchased from Fisher Chemical. All reagents were used as received without further purification, and Silicone cover stranded-core wires, and the Cu tapes (CST5) were purchased from Adafruit and Digi-Key.

Organohydrogel Synthesis: A total of 4 mL each of DI water and ethylene glycol were combined with 1 g of PVA and heated to 95 °C until fully

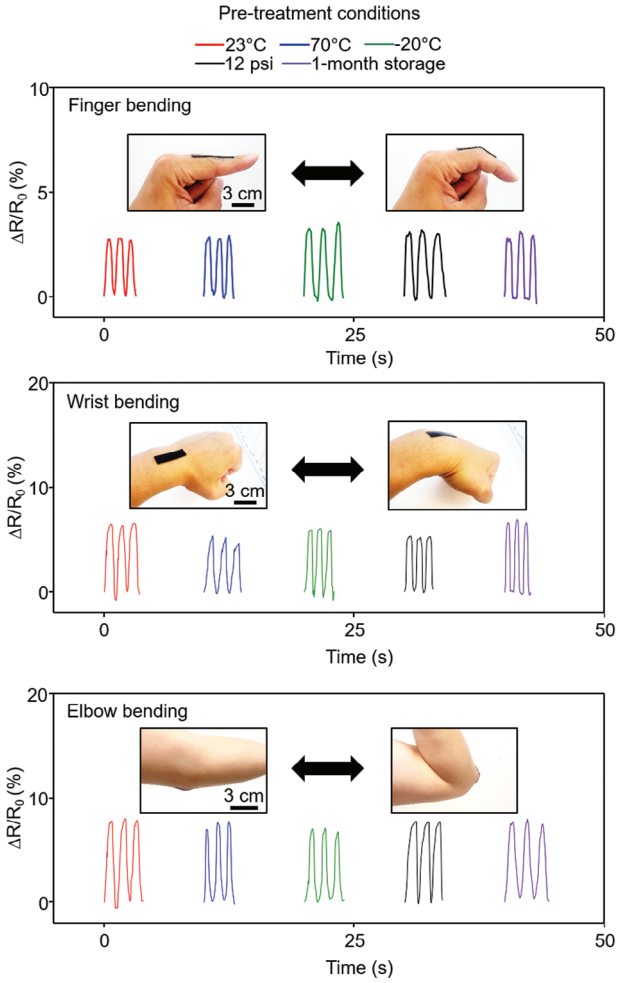

Figure 5. Proof-of-concept demonstrations in wearable sensing. Strain sensing results from various joints movement under varied environments.

dissolved. The resultant PVA solution was thoroughly mixed with 1 g of PEDOT:PSS solution for over 2 h. Subsequently, 2 mL of glycerol was integrated into the PVA-PEDOT:PSS solution, stirring continuously for another 2 h until a homogeneous solution was achieved. To ensure the uniformity of the solution, a QSONICA probe was employed for sonication. The probe, immersed in the solution, emitted ultrasonic waves, facilitating the breakup of any agglomerates and ensuring a homogeneous distribution. Post-sonication, the solution was meticulously poured into a pre-cleaned mold, taking care to avoid air bubble introduction. Once poured, the solution was left undisturbed at room temperature for at least 10 min, allowing it to conform to the mold shape and for any air bubbles to naturally dissipate. The mold was then securely sealed with a pre-cleaned glass cover to maintain sterility and protect the solution during subsequent steps. Prior to use, the mold and glass cover were cleaned with acetone, isopropanol, and deionized water to avoid contamination. Following this careful molding process, the solution underwent a freeze-thawing process to enhance its mechanical robustness. The organohydrogel was frozen overnight at −20 °C, then thawed at 25 °C for 3 h. Post-thaw, the specimen was carefully extracted from the mold and trimmed to the desired shape.

Dry Annealing Process: The dry annealing process started by positioning the trimmed freeze-thawed specimen between two glass substrates and subjecting it to dry annealing at 60 °C for more than an hour. After this initial annealing, one of the glass substrates was removed, exposing one side of the specimen for further annealing. This process was repeated multiple times, ensuring complete dry annealing of the entire specimen. The whole dry annealing process was conducted overnight.

Lyophilization and Structural Analysis: The organohydrogels underwent a 48 h lyophilization process with a Scientific Pro Freeze Dryer (HR7000-M; Harvestright, LLC.). Subsequently, their structural intricacies were examined using a high-resolution SEM (S-4800; Hitachi, Inc.).

Mechanical and Electrical Characterizations: Mechanical properties of the organohydrogel were determined by mechanical testing system (Mark-10) to obtain its stress–strain curve. The stress was determined by dividing the applied force by the initial cross-sectional area of the specimen. The strain was calculated as the change in length divided by the original length of the samples. The elastic modulus was determined from the initial linear slope of the stress-strain curve. The toughness was obtained by integrating the area under the stress-strain curve. The dissipated energy (U_{hys}) was estimated from the area enclosed by the stress–strain curves. The resistance of the organohydrogel was measured using a source meter (Keithley 2400; Tektronix, Inc.) in a two-wire configuration for electrical testing. Gauge factor (GF) was defined by the following Equation (1):

$$GF = (\Delta R/R_0)/\epsilon \quad (1)$$

where R_0, ΔR, and ϵ are the initial resistance before stretching, difference of resistance under stretching, and applied strain, respectively. To prepare for mechanical and electrical tests under different conditions, the organohydrogels underwent varied environments. Specifically, they were exposed to temperatures of either −20 or 70 °C, subjected to a vacuum of 12 psi for 12 h, and stored in the air for one month immediately before conducting the experiments at room temperature. Regarding the temperature condition of 70 °C, the samples were first stored at this temperature for one hour, and then they were placed between the glasses for the remaining duration of the experiment.

Human Motion Detection: All the human studies were conducted in compliance with the university regulations and approved by the Institutional Review Board (IRB protocol #: 202212-009-3). Silicone cover stranded-core wires (adafruit, Inc.) and Cu tapes (CST5) were attached to both sides of the hydrogel to serve as electrical connectors, after which the organohydrogel was mounted on the skin of various body parts. In the process of measuring, the wires were connected to a source meter (Keithley 2400; Tektronix, Inc.) in a two-wire configuration. In order to assess the sensing performance in diverse environments, the organohydrogels were subjected to storage under various conditions. The organohydrogels were put in very cold and hot temperatures (−20 and 70 °C), a vacuum of 12 psi for 12 h, and they were left in ambient conditions for one month. Regarding the temperature condition of 70 °C, the samples were placed at this temperature for one hour and then positioned between the glasses for the remaining duration of the experiment. Right after being stored, the specimens were affixed to the volunteer's joints to monitor human motion at room temperature.

Skin Irritation Testing: Hyperspectral line-scan images (hypercube) of human skin were captured to investigate inflammation, typically characterized by erythema and alterations in hemoglobin concentrations, following skin irritation.[16] Imaging was facilitated by a monochrome camera (GS3-U3-120S6M-C; FLIR) equipped with a 23 µm wide slit and a groove density of 150 mm^{-1}. Illumination was provided by an LED light source with a color temperature of 6500 K (D65). Spectrograph calibration was accomplished using a xenon light source, which emitted multiple narrow peaks at specific wavelengths. A fixed focal length lens (MVL25M1; Navitar) was primarily utilized to image the skin, achieving a field of view as small as 10 mm × 10 mm. RGB images of the same area were taken using a smartphone camera (iPhone 11 Pro; Apple). The organohydrogel was applied to the medial antebrachial cutaneous region of the forearm for ≈10 min, while a 3 M tape was attached to the same area for 10 min as a positive control. Images were captured before and after the experiment to enable a comparison of hemoglobin content. A mechanical linear scan step was executed at 0.25 mm increments, and data was collected using a custom MATLAB interface. To extract vital hemodynamic parameters from the hyperspectral image, a tissue reflectance spectral model was applied. Light propagation in the tissue was modeled using the theory of radiative

transport and robust approximations such as diffusion, Born, and empirical modeling. The intensity reflected from a biological sample can be represented as a function of λ in the visible range.

$$I_R(\lambda) = \left[b_1 \left(\frac{\lambda}{\lambda_0} \right)^{b_2} + b_3 \left(\frac{\lambda}{\lambda_0} \right)^{-4} \right] \exp \left[-b_4 \times \left\{ b_5 \times \varepsilon_{HbO_2}(\lambda) + (1 - b_5) \times \varepsilon_{Hb}(\lambda) \right\} \right] \quad (2)$$

where b_1, b_2, and b_3 are associated with the scattering (Mie or Rayleigh) contributions at $\lambda_0 = 800$ nm, ϵ_{HbO2} (λ) denotes the absorption coefficient of oxygenated hemoglobin (HbO_2), ϵ_{Hb} (λ) denotes the absorption coefficient of deoxygenated hemoglobin (H_b), b_4 is the hemoglobin concentration multiplied by the optical pathlength, and b_5 is the blood oxygen saturation (sPO_2). In the study, the hemoglobin contents multiplied by the optical pathlength (b_4) was used to indicate the level of skin irritation by Equation (2). All fitting parameters were computed using the simplex search (Nelder-Mead) algorithm.

Statistical Analysis: Data are presented as mean values ± standard deviation with a sample size of n = 3–4, as specified in the experiments. Statistical analysis was conducted using Origin Software.

Participant Recruitments: All human studies were conducted in compliance with university regulations and received approval from the Institutional Review Board. All participants voluntarily took part in the experiments after providing informed consent.

Supporting Information

Supporting Information is available from the Wiley Online Library or from the author.

Acknowledgements

This work was funded by the Eli Lilly and Company. C.H.L. acknowledges the Leslie A. Geddes Endowment at Purdue University. J.L. acknowledges the funding support from the MOTIE (Ministry of Trade, Industry, and Energy) in Korea, under the Human Resource Development Program for Industrial Innovation (Global) (P0017306, Global Human Resource Development for Innovative Design in Robot and Engineering) supervised by the Korea Institute for Advancement of Technology (KIAT). D.R.K. acknowledges funding support from the Basic Science Research Program (NRF-2021R1A2C1011418) through the National Research Foundation of Korea (NRF) funded by the Ministry of Science and ICT of Korea.

Conflict of Interest

The authors declare no conflict of interest.

Data Availability Statement

The data that support the findings of this study are available from the corresponding author upon reasonable request.

Keywords

dry annealing process, extreme environmental resistance, mechanical strength and stretchability, tough organohydrogel, wearable sensing applications

Received: August 25, 2023
Revised: October 30, 2023
Published online:

[1] a) C. Wang, X. Chen, L. Wang, M. Makihata, H.-C. Liu, T. Zhou, X. Zhao, *Science* **2022**, *377*, 517; b) T. Zhou, H. Yuk, F. Hu, J. Wu, F. Tian, H. Roh, Z. Shen, G. Gu, J. Xu, B. Lu, *Nat. Mater.* **2023**, 1; c) Y. Liu, J. Liu, S. Chen, T. Lei, Y. Kim, S. Niu, H. Wang, X. Wang, A. M. Foudeh, J. B.-H. Tok, *Nat Biomed Eng* **2019**, *3*, 58; d) J. C. Yang, J. Mun, S. Y. Kwon, S. Park, Z. Bao, S. Park, *Adv. Mater.* **2019**, *31*, 1904765; e) J. Park, J. Y. Kim, J. H. Heo, Y. Kim, S. A. Kim, K. Park, Y. Lee, Y. Jin, S. R. Shin, D. W. Kim, *Adv. Sci.* **2023**, *10*, 2207237; f) G. Zhang, J. Steck, J. Kim, C. H. Ahn, Z. Suo, *Sci. Adv.* **2023**, *9*, eadh7742; g) Y. Zhu, R. Haghniaz, M. C. Hartel, L. Mou, X. Tian, P. R. Garrido, Z. Wu, T. Hao, S. Guan, S. Ahadian, *ACS Biomater. Sci. Eng.* **2021**, *9*, 2048.

[2] a) C.-C. Kim, H.-H. Lee, K. H. Oh, J.-Y. Sun, *Science* **2016**, *353*, 682; b) X. P. Morelle, W. R. Illeperuma, K. Tian, R. Bai, Z. Suo, J. J. Vlassak, *Adv. Mater.* **2018**, *30*, 1801541; c) K. Lei, M. Chen, P. Guo, J. Fang, J. Zhang, X. Liu, W. Wang, Y. Li, Z. Hu, Y. Ma, *Adv. Funct. Mater.* **2023**, 2303511; d) H. Liao, X. Guo, P. Wan, G. Yu, *Adv. Funct. Mater.* **2019**, *29*, 1904507; e) L. Han, K. Liu, M. Wang, K. Wang, L. Fang, H. Chen, J. Zhou, X. Lu, *Adv. Funct. Mater.* **2018**, *28*, 1704195; f) Y. Jian, S. Handschuh-Wang, J. Zhang, W. Lu, X. Zhou, T. Chen, *Mater. Horiz.* **2021**, *8*, 351.

[3] a) Q. Zhou, J. Lyu, G. Wang, M. Robertson, Z. Qiang, B. Sun, C. Ye, M. Zhu, *Adv. Funct. Mater.* **2021**, *31*, 2104536; b) H. Yuk, T. Zhang, G. A. Parada, X. Liu, X. Zhao, *Nat. Commun.* **2016**, *7*, 12028.

[4] Y.-F. Zhang, M.-M. Guo, Y. Zhang, C. Y. Tang, C. Jiang, Y. Dong, W.-C. Law, F.-P. Du, *Polym. Test.* **2020**, *81*, 106213.

[5] Z. Liu, J. Zhang, J. Liu, Y. Long, L. Fang, Q. Wang, T. Liu, *J. Mater. Chem. A* **2020**, *8*, 6219.

[6] a) Z. Shen, Z. Zhang, N. Zhang, J. Li, P. Zhou, F. Hu, Y. Rong, B. Lu, G. Gu, *Adv. Mater.* **2022**, *34*, 2203650. b) Q. Zhao, J. Liu, Z. Wu, X. Xu, H. Ma, J. Hou, Q. Xu, R. Yang, K. Zhnag, M. Zhang, H. Yang, W. Peng, X. Liu, C. Zhang, J. Xu, B. Lu, *Chem. Eng. J.* **2022**, *442*, 136284. c) A. Prameswati, S. A. Nurmaulia Entifar, J. W. Han, A. F. Wibowo, J. H. Kim, Y. S. b. Sembiring, J. Park, J. Lee, A.-Y. Lee, M. H. Song, S. Kim, D. C. Lim, Y. Eom, S. Heo, M.-W. Moon, M.-S Kim, Y. H. Kim, *ACS Appl. Mater. Interfaces* **2023**, *15*, 24648

[7] Y. Chen, J. Li, J. Lu, M. Ding, Y. Chen, *Polym. Test.* **2022**, *108*, 107516.

[8] a) Y. Liu, J. Yin, Y. Fu, P. Zhao, Y. Zhang, B. He, P. He, *Chem. Eng. J.* **2020**, *382*, 122925; b) Z. Wang, J. Chen, L. Wang, G. Gao, Y. Zhou, R. Wang, T. Xu, J. Yin, J. Fu, *J. Mater. Chem. B* **2019**, *7*, 24; c) Y. Ma, Y. Gao, L. Liu, X. Ren, G. Gao, *Chem. Mater.* **2020**, *32*, 8938. d) Y. Zhou, C. Wan, Y. Yang, H. Yang, S. Wang, Z. Dai, K. Ji, H. Jiang, X. Chen, Y. Long, *Adv. Funct. Mater.* **2019**, *29*, 1806220. e) J. Wei, Q. Wang, *Small Methods* **2019**, *3*, 1900558.

[9] G. Li, K. Huang, J. Deng, M. Guo, M. Cai, Y. Zhang, C. F. Guo, *Adv. Mater.* **2022**, *34*, 2200261.

[10] a) J. T. Muth, D. M. Vogt, R. L. Truby, Y. Mengüç, D. B. Kolesky, R. J. Wood, J. A. Lewis, *Adv. Mater.* **2014**, *26*, 6307; b) J. Yuan, Y. Zhang, G. Li, S. Liu, R. Zhu, *Adv. Funct. Mater.* **2022**, *32*, 2204878; c) A. Chhetry, S. Sharma, S. C. Barman, H. Yoon, S. Ko, C. Park, S. Yoon, H. Kim, J. Y. Park, *Adv. Funct. Mater.* **2021**, *31*, 2007661; d) Y. Lu, X. Qu, W. Zhao, Y. Ren, W. Si, W. Wang, Q. Wang, W. Huang, X. Dong, *J Reticuloendothel Soc* **2020**, 2020; e) K.-H. Kim, S. K. Hong, S.-H. Ha, L. Li, H. W. Lee, J.-M. Kim, *Mater. Horiz.* **2020**, *7*, 2662; f) S. Wu, S. Peng, Z. J. Han, H. Zhu, C. H. Wang, *ACS Appl. Mater. Interfaces* **2018**, *10*, 36312.

[11] a) C. Ma, M. G. Ma, C. Si, X. X. Ji, P. Wan, *Adv. Funct. Mater.* **2021**, *31*, 2009524; b) G. Li, C. Li, G. Li, D. Yu, Z. Song, H. Wang, X. Liu, H. Liu, W. Liu, *Small* **2022**, *18*, 2101518.

[12] C. Tan, Z. Dong, Y. Li, H. Zhao, X. Huang, Z. Zhou, J.-W. Jiang, Y.-Z. Long, P. Jiang, T.-Y. Zhang, *Nat. Commun.* **2020**, *11*, 3530.

[13] N. Qaiser, F. Al-Modaf, S. M. Khan, S. F. Shaikh, N. El-Atab, M. M. Hussain, *Adv. Funct. Mater.* **2021**, *31*, 2103375.

[14] M. Amit, L. Chukoskie, A. J. Skalsky, H. Garudadri, T. N. Ng, *Adv. Funct. Mater.* **2020**, *30*, 1905241.

[15] a) M. Zarei, G. Lee, S. G. Lee, K. Cho, *Adv. Mater.* **2023**, *35*, 2203193; b) W. Li, J. Liu, J. Wei, Z. Yang, C. Ren, B. Li, *Adv. Funct. Mater.* **2023**, *33*, 2213485; c) Y. Niu, H. Liu, R. He, M. Luo, M. Shu, F. Xu, *Small* **2021**, *17*, 2101151; d) A. J. Cheng, L. Wu, Z. Sha, W. Chang, D. Chu, C. H. Wang, S. Peng, *Adv. Mater. Technol.* **2023**, *8*, 2201959.

[16] a) Y. Ji, S. M. Park, S. Kwon, J. W. Leem, V. V. Nair, Y. Tong, Y. L. Kim, *PNAS Nexus* **2023**, *2*, pgad111; b) G. D. de Melo, F. Lazarini, S. Levallois, C. Hautefort, V. Michel, F. Larrous, B. Verillaud, C. Aparicio, S. Wagner, G. Gheusi, *Sci. Transl. Med.* **2021**, *13*, eabf8396.